

NAVAL POSTGRADUATE SCHOOL Monterey, California



THESIS

**RADAR CROSS SECTION REDUCTION:
GEOMETRIC CONTROL OF DISCONTINUITIES
USING SERRATED EDGES**

by

Matthew K. M. Yong

March 1998

Thesis Advisor:
Second Reader:

David C. Jenn
Phillip E. Pace

Approved for public release; distribution is unlimited.

DTIC QUALITY INSPECTED 2

19980514 090

REPORT DOCUMENTATION PAGE

Form Approved
OMB No. 0704-0188

Public reporting burden for this collection of information is estimated to average 1 hour per response, including the time for reviewing instruction, searching existing data sources, gathering and maintaining the data needed, and completing and reviewing the collection of information. Send comments regarding this burden estimate or any other aspect of this collection of information, including suggestions for reducing this burden, to Washington headquarters Services, Directorate for Information Operations and Reports, 1215 Jefferson Davis Highway, Suite 1204, Arlington, VA 22202-4302, and to the Office of Management and Budget, Paperwork Reduction Project (0704-0188) Washington DC 20503.

1. AGENCY USE ONLY (Leave blank)

2. REPORT DATE

March 1998

3. REPORT TYPE AND DATES COVERED

Master's Thesis

4. TITLE AND SUBTITLE

RADAR CROSS SECTION REDUCTION: GEOMETRIC CONTROL OF DISCONTINUITIES USING SERRATED EDGES

5. FUNDING NUMBERS

6. AUTHOR(S)

Yong, Matthew K. M.

7. PERFORMING ORGANIZATION NAME(S) AND ADDRESS(ES)

Naval Postgraduate School
Monterey, CA 93943-5000

8. PERFORMING ORGANIZATION REPORT NUMBER

9. SPONSORING / MONITORING AGENCY NAME(S) AND ADDRESS(ES)

10. SPONSORING / MONITORING AGENCY REPORT NUMBER

11. SUPPLEMENTARY NOTES

The views expressed in this thesis are those of the author and do not reflect the official policy or position of the Department of Defense or the U.S. Government.

12a. DISTRIBUTION / AVAILABILITY STATEMENT

Approved for public release; distribution is unlimited.

12b. DISTRIBUTION CODE

13. ABSTRACT (maximum 200 words)

The objective of this thesis is to investigate and evaluate the effectiveness of radar cross section (RCS) reduction by means of the geometric control of discontinuities using serrated edges. Although the use of serrated edges for RCS reduction can be clearly seen on stealth aircraft such as the Northrop B-2, and was mentioned in several papers and references, not much data on the reduction magnitude, the associated geometry, or the design methodology are available in the open literature. Parameters of interest include the number of basic serration cells (triangles) required per wavelength, and the aspect ratio of the triangles that form the zig zags. An infinitely thin metallic plate is considered for the analysis. The RCS of such a plate with serrated edges is computed and compared against the RCS of a plate of the same sized without serrated edges. The infinitely thin assumption is valid if the wing of the aircraft, which is represented by the plate, is thin compared to the wavelength. The results obtained show significant reduction in RCS.

14. SUBJECT TERMS

RCS, edges diffraction, method of moments

15. NUMBER OF PAGES

60

16. PRICE CODE

17. SECURITY CLASSIFICATION OF REPORT

Unclassified

18. SECURITY CLASSIFICATION OF THIS PAGE

Unclassified

19. SECURITY CLASSIFICATION OF ABSTRACT

Unclassified

20. LIMITATION OF ABSTRACT

UL

Approved for public release; distribution is unlimited.

**RADAR CROSS SECTION REDUCTION:
GEOMETRIC CONTROL OF DISCONTINUITIES
USING SERRATED EDGES**

Matthew K. M. Yong
Ministry of Defence, Singapore
B. Eng., University of Surrey, UK, 1990

Submitted in partial fulfillment
of the requirements for the degree of

MASTER OF SCIENCE IN ELECTRICAL ENGINEERING

from the

**NAVAL POSTGRADUATE SCHOOL
March 1998**



Author:

Matthew K. M. Yong

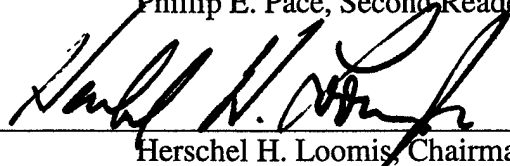
Approved by:



David C. Jenn, Thesis Advisor



Phillip E. Pace, Second Reader



Herschel H. Loomis, Chairman
Department of Electrical and Computer Engineering

ABSTRACT

The objective of this thesis is to investigate and evaluate the effectiveness of radar cross section (RCS) reduction by means of the geometric control of discontinuities using serrated edges. Although the use of serrated edges for RCS reduction can be clearly seen on stealth aircraft such as the Northrop B-2, and was mentioned in several papers and references, not much data on the reduction magnitude, the associated geometry, or the design methodology are available in the open literature. Parameters of interest include the number of basic serration cells (triangles) required per wavelength, and the aspect ratio of the triangles that form the zig zags. An infinitely thin metallic plate is considered for the analysis. The RCS of such a plate with serrated edges is computed and compared against the RCS of a plate of the same sized without serrated edges. The infinitely thin assumption is valid if the wing of the aircraft, which is represented by the plate, is thin compared to the wavelength. The results obtained show significant reduction in RCS.

TABLE OF CONTENTS

I.	INTRODUCTION	1
II.	NON-SPECULAR SCATTERING	7
	A. SURFACE WAVES	7
	B. DIFFRACTION	9
	C. RCS TREATMENT	10
	1. Impedance Matching	10
	2. Absorber	11
	3. Geometric Control	12
III.	APPROXIMATE HIGH-FREQUENCY EDGE DIFFRACTION TECHNIQUES	13
	A. GTD	14
	B. THE METHOD OF EQUIVALENT CURRENTS	16
	C. PTD	18
IV.	COMPUTER CODES	21
	A. PATCH	21
	1. Method of Moments	21
	2. PATCH Input	24
	3. PATCH Code Capabilities	24
	B. ACAD	25
V.	RESULTS AND ANALYSIS	29
	A. SINGLE-EDGE SERRATED PLATE	30
	B. DOUBLE-EDGE SERRATED PLATE	38

VI. CONCLUSIONS43

LIST OF REFERENCES47

INITIAL DISTRIBUTION LIST49

ACKNOWLEDGMENT

I would like to acknowledge my thesis advisor, Professor David C. Jenn for his guidance and encouragement.

Most of all, I would like to thank my wife, Selina and my daughter, Grace for their love, support and understanding.

I. INTRODUCTION

The development of increasingly sophisticated detection systems threatens to reduce the mission effectiveness of many types of weapons platforms. Much effort has been focused on methods of increasing survivability by reducing detectability. Low observable (LO) platform design has therefore become an important engineering task over the last several decades. Although the principles of radar stealth are well known, radar cross section (RCS) prediction and reduction are still difficult tasks.

In general, four basic techniques are employed in radar cross section reduction:

1. shaping,
2. surface material selection,
3. active cancellation, and
4. passive cancellation.

Shaping is typically the primary means of RCS reduction. However, RCS reduction at one viewing angle and frequency is usually accompanied by an enhancement at other viewing angles and frequencies. Surface material selection requires the addition of lossy materials (radar absorbing material) to the surface of the target. RCS reduction for this case is achieved by the dissipation of energy inside of the material. The performance of the platform (e.g., aerodynamic efficiency) generally decreases due to added

weight. Active cancellation refers to methods of reproducing a signal that is 180° out of phase from the target's skin return so that the total scattered field is zero. Passive cancellation is the addition of a secondary scatterer to cancel the reflected field from the primary target. Active and passive cancellation techniques are usually limited to narrow frequency bands and spatial regions.

The RCS of an object can be attributed to a combination of specular and non-specular scattering components. Specular scatterers refer to any part of an object where surfaces are relatively flat in terms of wavelength and, in the case of monostatic RCS, perpendicular to the incident electromagnetic wave. A flat and smooth surface is a very strong scatterer at normal incidence, but the echo reduces rapidly as the angle of incidence moves away from the surface normal. The larger the surface area in terms of wavelength, the higher the maximum RCS, and the narrower the angular region of the lobe.

Specular scattering is usually reduced by shaping. With proper orientation of specular surfaces, the scattered energy can be deflected away from the threat sector. This leads to the design of unconventional platform structures. In the case of aircraft, the design of a faceted airframe drastically reduces the number of specular directions for

which large RCS echoes will be observed. However, this will also create a multitude of edges.

Edges are important constituents in three different types of scattering. First, there is an edge diffraction return due a leading edge for parallel polarization or a trailing edge for perpendicular polarization. Diffraction can be defined as any non-specular scattering of energy due to edges and vertices. Next, edges provide the source from which physical optics end-region return arises. End-region scattering is due to physical optics like currents at edges referred to as fringe currents. Finally, edges also provide discontinuities that reflect surface traveling waves, potentially resulting in a strong return in the backscattering direction. Surface waves are generated by current waves that flow across the surface and are scattered by trailing edges.

Edge return becomes important when high level specular scattering is eliminated, which is the case for low observable platforms. Further RCS reduction may be possible by the geometric control of edges. A serrated edge may cause diffraction and back-scattering to be dispersed in other directions, thereby reducing the RCS in the threat sector. Serrated edge treatment may be applied to the leading and trailing edges of wings. Obvious examples are the Northrop B-2 and the Lockheed F-117A aircraft shown in Figure 1 and

Figure 2, where the trailing-edge zig zags are clearly visible.

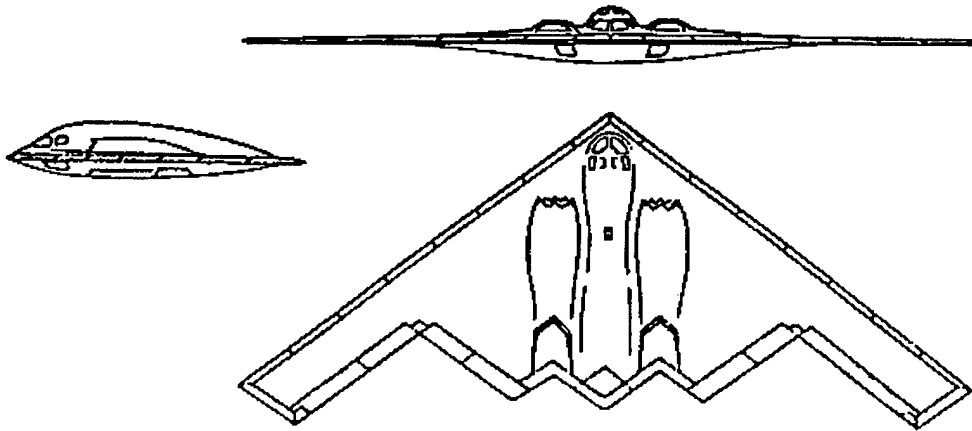


Figure 1. The Northrop B-2 (from [1]).

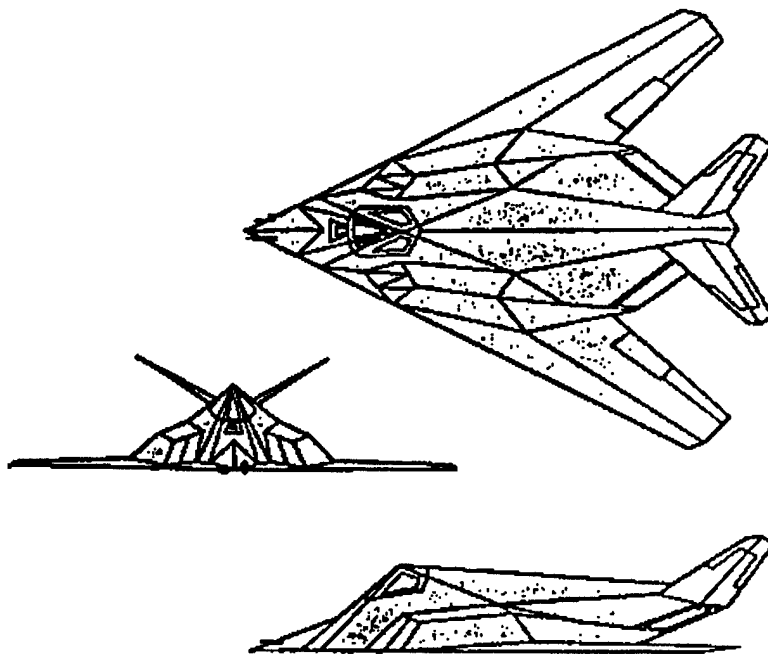


Figure 2. The Lockheed F-117A (from [1]).

It would be desirable if design guidance based on the above scattering mechanisms of edges could be provided by an analytical approach. However, no such approach currently exist. The objective of this thesis is to investigate and evaluate the effectiveness of RCS reduction by means of the geometric control of discontinuities with serrated edges.

Chapter II discusses two major scattering mechanisms related to edges. The concepts of surface traveling waves and edge diffraction are explained. Chapter III introduces three high-frequency techniques commonly used to compute the scattering from metallic edges. They are the geometrical theory of diffraction, the physical theory of diffraction and the method of equivalent currents. Chapter IV contains a description of the software codes that were used in this thesis. The method of moments and its corresponding implementation in the computer codes is also discussed. Chapter V presents the data and the analysis of the results. Finally, Chapter VI presents the conclusions and recommendations for future work.

II. NON-SPECULAR SCATTERING

A. SURFACE WAVES

Propagation mechanisms that occur at an interface between two different media are generally referred to as *surface waves*. Surface waves are important in the absence of high level specular scattering, as in the case of low observable platforms. Surface waves are non-specular; that is, the maximum scattering does not occur for the angle of observation equal to the angle of incidence. Their RCS is independent of body area but proportional to L/λ^2 , where L is the length of the surface over which the wave travels and λ is the wavelength of the incident ray [1].

A surface wave that propagates with little or no attenuation is termed as *traveling wave*. If the surface is terminated with a discontinuity such as an edge, the traveling wave will be reflected back toward its origin. For an electric conductor, a traveling wave occurs only when the incident electric field has component perpendicular to the surface and in the plane of incidence. The plane of incidence is defined by the direction of incidence \hat{k} and the surface normal \hat{n} , as shown in Figure 3, where \vec{E}_i and \vec{H}_i are the incident field intensities. This polarization is defined as transverse magnetic to \hat{z} (TM_z) because the

magnetic field intensity vector \vec{H}_i , is transverse to the z -axis. If there is not electric field component in the plane of incidence, there will not be traveling wave for an electric conductor.

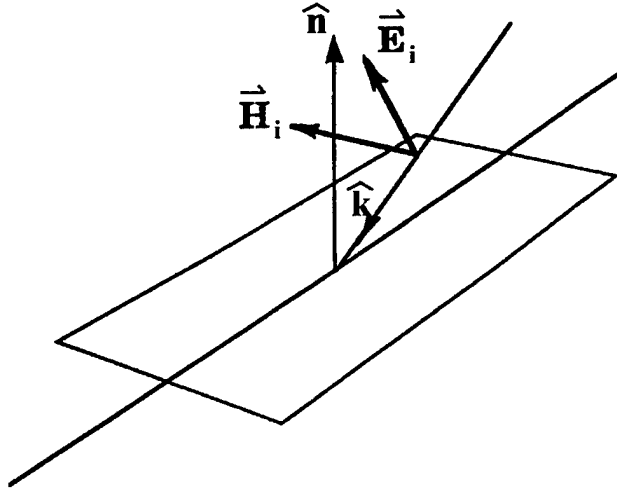


Figure 3. Incident electric field with components perpendicular and parallel to the surface in the plane of incidence (after [2]).

For a traveling wave, the illuminated target acts as a combination of antenna and transmission line, collecting incident energy and guiding it along the surface until an edge or load is encountered. The edge in turn generates backward-traveling wave with significant backscattering echo. The magnitude of the reflected echo of the surface traveling wave depends on the size and shape of the edge and on the angle of arrival with respect to the edge. In the case of aircraft, a surface traveling wave excites the

trailing edges of the wings and horizontal stabilizers when the incident waves are vertically polarized. The leading edges also support traveling wave for horizontally polarized waves if the angle of incidence is within 20° to 30° from the edge [2].

B. DIFFRACTION

When an electromagnetic ray impinges on a finite flat surface, part of the wave is scattered by the surface and part by the edge itself. These so-called edge diffracted rays will propagate in all directions perpendicular to the edge if the incident wave is normal to the edge. For non-normal incidence, an edge-diffracted ray can lie anywhere along a forward cone whose half-angle is subtended by the edge and the incident ray. This is commonly known as the Keller cone after J. B. Keller, shown in Figure 4, where β_i and β_s are the angles between the edge and the incident and the scattering rays, respectively.

In contrast to the ray optics description of edge diffraction, it can also be viewed as a disturbance of the current near the leading and trailing edges. If one could determine the fringe current (i.e., the change in current due to the presence of the edge), then it could be used in the radiation integrals to compute the edge-scattered field.

This later view is a current based approach to edge diffraction.

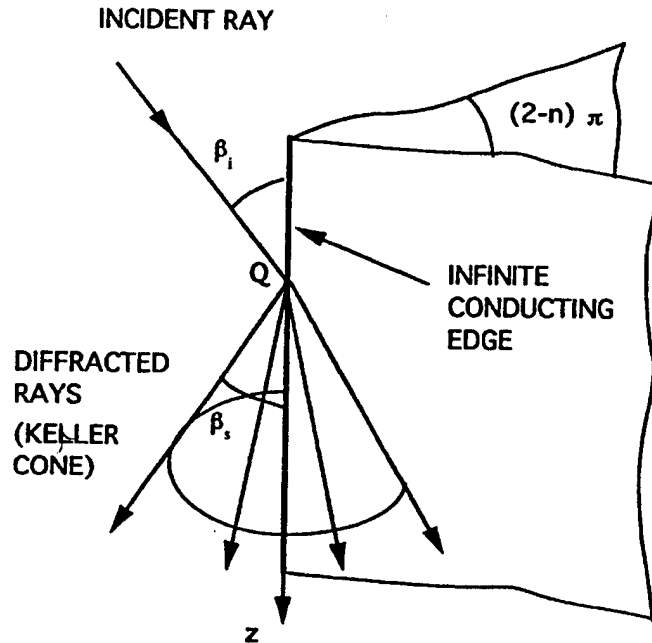


Figure 4. Diffracted ray geometry and the Keller cone (after [1]).

C. RCS TREATMENT

1. Impedance Matching

The reflection and re-radiation due to surface waves can be eliminated from the threat direction by matching the terminating edges. This is usually a narrowband approach based on the impedance transformation concept similar to that used in transmission line matching. An illustration of

terminal matching to remove the traveling wave is shown in Figure 5.

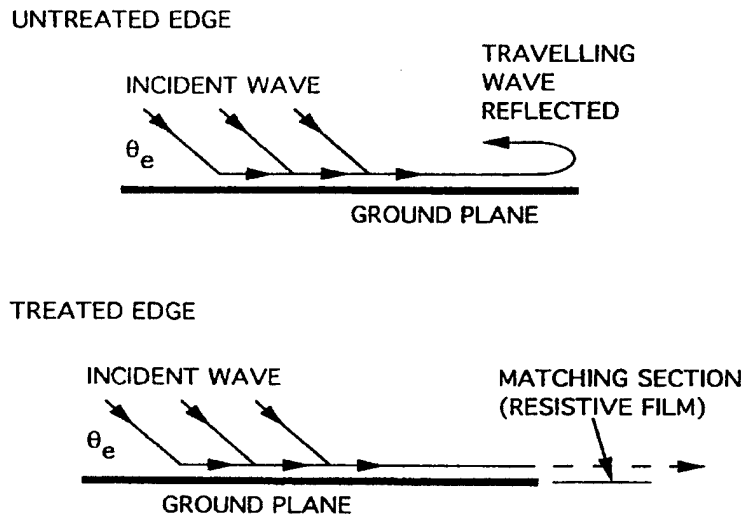


Figure 5. Matching a edge with a resistive strip (from [1]).

A second discontinuity is added with its characteristics adjusted such that its scattered field cancels with that of the original discontinuity. Similar to the transmission line matching, the length of the matching section is about 0.25λ . The corresponding resistivity value can be determined using the method of moments (a computational technique which will be introduced later in Chapter IV).

2. Absorber

Another effective and popular method of suppressing surface traveling waves is to apply absorbers. Although the

attenuation provided by these absorbers is typically limited, the backward scattering traveling wave must travel the surface twice, and hence the loss provided by the absorbers will be doubled. The disadvantage of adding absorbers is the decrease in performance of the platform (e.g., aerodynamic efficiency) due to additional weight and bulk.

3. Geometric Control

In some cases, it is possible to tilt the axis of an edge so that its high RCS is out of the threat sector. Serration is a geometric treatment that can be applied to the leading and trailing edges of an aircraft's wings. Examples of such implementation can be seen on the wings of the Northrop B-2, as shown earlier in Figure 1. Serrated edges can also be found on the weapon bay doors and landing-gear bay doors of LO aircraft. The effectiveness of RCS reduction using geometric control of discontinuities with serrated edges is presented and analyzed in Chapter V.

III. APPROXIMATE HIGH-FREQUENCY EDGE DIFFRACTION TECHNIQUES

This chapter presents an overview of the three most commonly used high-frequency edge diffraction techniques. The term "*high-frequency*" does not refer to the actual frequency of the incident wave, but to the size of the target when compared to the incident wavelength.

Geometrical optics (GO) and physical optics (PO) are among the oldest and most popular high-frequency methods used for estimating the RCS of an object. The theory of GO was based on the early studies of light and uses simple formulas involving the local radii of curvature at the specular point. This simple approach fails when the radii of curvature become infinite. The theory of PO overcomes this limitation by approximating the induced surface currents as a function of the incident field and integrating them to obtain the scattered fields. The PO approximation holds provided that the surface is relatively large and the scattering direction is not too far from the specular direction. The PO approximation fails at wide angles from the specular direction because the contribution from the edge is not modeled exactly.

Over the years, high-frequency diffraction techniques such as the geometrical theory of diffraction (GTD), the physical theory of diffraction (PTD) and the method of equivalent currents have been developed to calculate the

diffraction effects of metallic edges. These techniques are applicable if the edges of the scattering body are long compared to the wavelength of the incident field.

A. GTD

GTD was introduced by Keller [3] as an asymptotic method for the solution of diffraction problems at high frequencies. It was developed to supplement geometrical optics. The total field at an observation point can be decomposed into GO and diffracted components:

$$\vec{E}_s = \vec{E}_{go} + \vec{E}_d. \quad (1)$$

The diffracted field is determined from a suitable canonical problem. A canonical problem is one that has the same local geometry features and for which a known scattered field is available. An infinite knife is an appropriate canonical problem for a thin plate edge. The problem of scattering from an infinite knife edge was solved analytically by Sommerfeld [11]. The diffracted electric field can be expressed as [2],

$$\vec{E}_d = \frac{-\Gamma e^{jks}}{\sin^3 \beta_i} [(\hat{t} \cdot \vec{E}_i)(X - Y)\hat{s} \times (\hat{s} \times \hat{t}) + Z_o(\hat{t} \cdot \vec{H}_i)(X + Y)\hat{s} \times \hat{t}] \quad (2)$$

where Γ is a divergence factor, $k = 2\pi/\lambda$ is the free-space wave number, s is the distance along the ray from the edge

element to a far field observation point, \hat{s} is the unit vector of this ray, β_i is the angle subtended by the edge and the incident ray as shown in Figure 4, and \hat{t} is a unit vector aligned along the edge. The diffraction coefficients are [2],

$$X = \frac{(1/n)\sin(\pi/n)}{\cos(\pi/n) - \cos[(\psi_s - \psi_i)/n]} \quad (3)$$

$$Y = \frac{(1/n)\sin(\pi/n)}{\cos(\pi/n) - \cos[(\psi_s + \psi_i)/n]}$$

where n is the exterior wedge angle normalized with respect to π , and ψ_i and ψ_s are the angles of the transverse components of the incident and diffracted directions with respect to one of the surfaces meeting at the edge, as shown in Figure 6.

GTD, like all ray tracing techniques, has the limitation of predicting infinite fields wherever an infinity of rays come together (these points or lines are referred to as caustics). This is obviously wrong since the far diffracted field must be finite in the real world. This problem requires some form of "caustic matching" correction which blends the wide-angle predictions smoothly into the known value of the caustic.

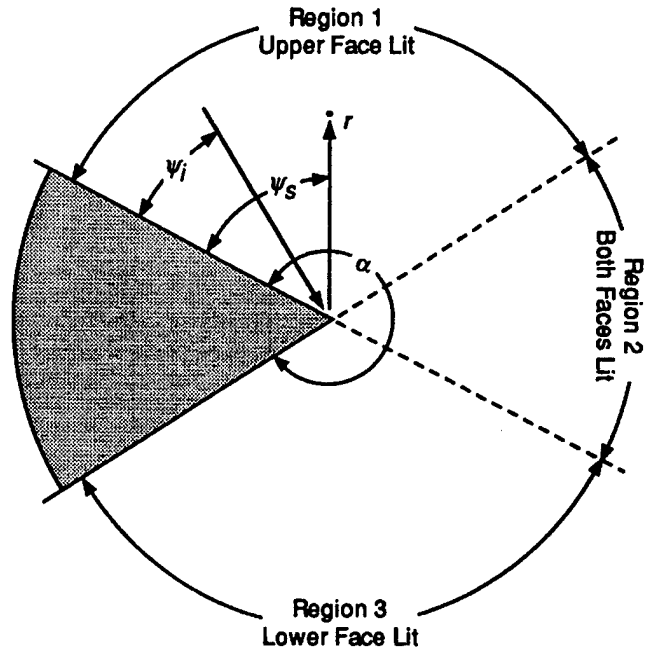


Figure 6. Geometry for wedge diffraction (from [2]).

B. THE METHOD OF EQUIVALENT CURRENTS

The axial caustic problem of GTD can be eliminated by the method of equivalent currents. Note that any finite current distribution produces a finite result for the far diffracted field when that distribution is summed in a radiation integral. In addition, the method of equivalent currents ensure that the diffracted fields can be computed for scattering directions out of the Keller cone.

The method of equivalent currents postulates that fictitious electric and magnetic current filaments flow

along the edges. The magnitude and phase of the electric and the magnetic currents as proposed by Michaeli are [4]:

$$I_e = \frac{j2(\hat{t} \cdot \vec{E}_i)D_e}{kZ_o \sin^2 \beta_i} + \frac{j2(\hat{t} \cdot \vec{H}_i)D_{em}}{k \sin^2 \beta_i} \quad (4)$$

$$I_m = -\frac{j2(\hat{t} \cdot \vec{H}_i)D_m}{kY_o \sin \beta_i \sin \beta_s} \quad (5)$$

where $Z_o = 1/Y_o$ is the free-space impedance. The diffraction coefficients D_e , D_m and D_{em} are [2, 4],

$$D_e = \frac{\frac{1}{n} \frac{\sin \psi_i}{n}}{\cos \frac{\pi - \alpha_1}{n} - \cos \frac{\psi_i}{n}} + \frac{\frac{1}{n} \frac{\sin \psi_i}{n}}{\cos \frac{\pi - \alpha_2}{n} - \cos \frac{\psi_i}{n}} \quad (6)$$

$$D_m = \frac{\sin \psi_s}{\sin \alpha_1} \cdot \frac{\frac{1}{n} \frac{\sin \frac{\pi - \alpha_1}{n}}{n}}{\cos \frac{\pi - \alpha_1}{n} - \cos \frac{\psi_i}{n}} + \frac{\sin(n\pi - \psi_s)}{\sin \alpha_2} \cdot \frac{\frac{1}{n} \frac{\sin \frac{\pi - \alpha_2}{n}}{n}}{\cos \frac{\pi - \alpha_2}{n} - \cos \frac{\psi_i}{n}} \quad (7)$$

$$D_{em} = \frac{Q}{\sin \beta_i} \left[\frac{\cos \psi_s}{\sin \alpha_1} \cdot \frac{\frac{1}{n} \frac{\sin \frac{\pi - \alpha_1}{n}}{n}}{\cos \frac{\pi - \alpha_1}{n} - \cos \frac{\psi_i}{n}} - \frac{\cos(n\pi - \psi_s)}{\sin \alpha_2} \cdot \frac{\frac{1}{n} \frac{\sin \frac{\pi - \alpha_2}{n}}{n}}{\cos \frac{\pi - \alpha_2}{n} - \cos \frac{\psi_i}{n}} \right] \quad (8)$$

with

$$Q = \sin \beta_s \cot \beta_i - \sin \beta_i \cot \beta_s \quad (9)$$

$$\sin \alpha_1 = \frac{[\sin^2 \beta_i - \sin^2 \beta_s \cos^2 \psi_s]^{1/2}}{\sin \beta_i} \quad (10)$$

and

$$\sin \alpha_2 = \frac{[\sin^2 \beta_i - \sin^2 \beta_s \cos^2 (n\pi - \psi_s)]^{1/2}}{\sin \beta_i} \quad (11)$$

With the method of equivalent currents proposed by Michaeli, edge-diffracted fields remain finite in caustic directions and the scattering direction is no longer confined to a generator of the Keller cone.

C. PTD

PTD is a current-based technique to obtain the edge scattered field of metallic bodies. It was developed by Ufimtsev based on a refinement of the physical optics (PO) approximation [10].

Ufimtsev postulates that the total induced surface current J_s , is the sum of the PO contribution J_{PO} , and an edge contribution J_f :

$$J_s = J_{PO} + J_f. \quad (12)$$

Ufimtsev refers to J_{PO} as the "uniform" current and J_f as the "non-uniform" current. If the non-uniform current is known, then the diffracted field due to the edge can be

calculated by integrating this current over the surface. However, the exact non-uniform current can only be determined by solving a boundary-value problem which is very complicated.

In order to obtain the edge-diffracted field, Ufimtsev subtracted the PO current from the total induced current, which can be determined from a canonical problem. The approximate canonical problem for edge scattering is an infinite knife edge. Using analytical methods, J_s is determined for the knife edge, then Equation (12) used to find the residue J_f which, finally, is used as an estimate for the fringe current on a finite edge.

Although PTD is simple in principle, it can be rather difficult to implement in practice. Complicated two-dimensional integration is often necessary as the fringe currents can extend quite a distance from the edge. In addition, a comprehensive theory for fringe current interaction has yet to be developed.

As a final comment, it can be shown that all of these high frequency diffraction techniques are equivalent [5]. That is, in the limit of increasing frequency, GTD and PTD give identical results. An advantage of these methods is that they provide some physical insight into the scattering from edges and can be used to predict the direction of maximum RCS. However, they are limited to long edges (in

terms of wavelength). For the serration geometries of interest in this research, which are in the order of 1λ or less, these methods are not suitable for computing low-level edge diffraction. A rigorous approach, such as the method of moments, should be used. The method of moments technique is discussed in the next chapter.

IV. COMPUTER CODES

A. PATCH

PATCH is a method of moments (MM) triangular subdomain code that was developed by Sandia Labs [6]. It is a FORTRAN computer code that computes electromagnetic scattering and radiation based on the MM solution of the E-field integral equation (EFIE). It models a continuous surface by discrete triangular patches in order to handle arbitrary shaped bodies easily and accurately. This chapter presents a brief summary of the method of moments and its implementation in PATCH.

1. Method of Moments

The method of moments reduces the EFIE to a set of linear equations that can be solved using standard matrix methods. The number of unknowns, and hence the size of the matrix equation that must be solved, depends on the number of triangular patches that are used to represent the scattering body. In general, the more triangles, the shorter the edge lengths and the more accurate the results. A useful rule of thumb is to limit the edge lengths to 0.1λ .

A surface or patch based method of moments solution is rigorous; that is, as the triangles become smaller, the method of moments solution converges to the correct value.

Unlike a wire simulation (wire grid model), the area between edges which form the triangle facets are solid material, not air gaps. Therefore, current truly flows on the surface of the object, not just along wires approximating the surface.

The unknown quantity in the EFIE is the surface current distribution \vec{J}_s . To apply the method of moments, \vec{J}_s is represented by a series of unknown coefficients

$$\vec{J}_s = \sum_{n=1}^N I_n \vec{J}_n \quad (13)$$

where $\{\vec{J}_n\}$ are the basis functions. Typical basis functions include pulses, δ functions, triangles and sinusoids. To determine the unknown coefficients $\{I_n\}$, a matrix of N linear equations is formed. By exploiting the properties of the basis functions, the $\{I_n\}$ are determined and thus \vec{J}_s is also determined. Once the current coefficients have been determined using the method of moments procedure, the radiation patterns and the scattered fields can be computed.

The application of the method of moments depends on the capability and capacity of the computer. Because of the edge length restriction for convergence, bodies with large number of triangles generate matrices that are too large for the computer or require processing time that are too long for practical application. In general, the number of edges and

unknowns (i.e., number of simultaneous equations that must be solved) is almost the same. Small differences occur due to the fact that there are more than two current coefficients associated with some edges. On the other hand, if the edge of a triangle is also the edge of the body, then there is no current flowing across it and therefore no expansion coefficient is required. PATCH uses overlapping rooftop functions for \vec{J}_n . The current at a point on a triangle is the vector sum of the currents crossing the edges weighted by their distances from the edge.

Several output files are generated by PATCH. They include the RCS as a function of the spherical angles θ and ϕ which are shown in Figure 7.

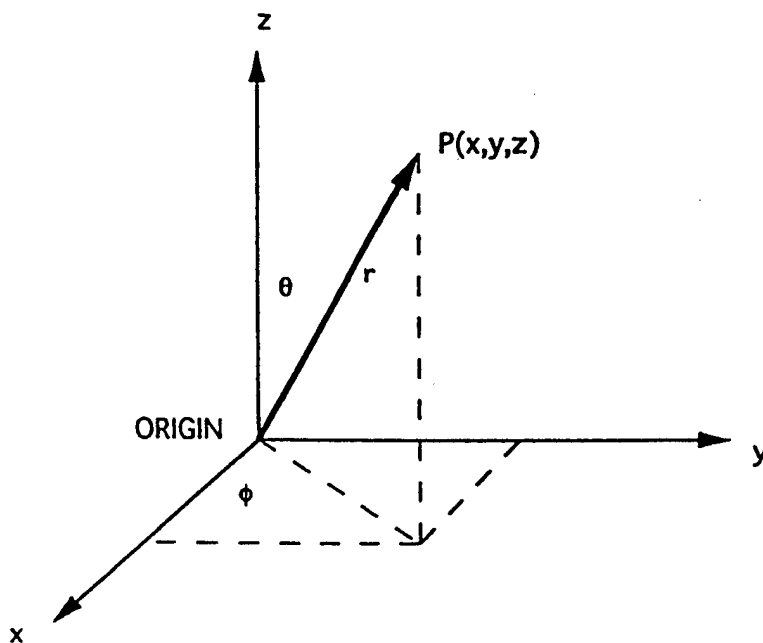


Figure 7. Spherical coordinate systems (from [1]).

2. PATCH Input

The input file for PATCH is an ASCII file that contains all of the geometry information and calculation parameters. The file can be generated using the preprocessing code BUILD that is distributed along with PATCH. BUILD is capable of generating basic geometrical shapes and combining them to yield more complex shapes. In addition to geometry information, BUILD also prompts the user for calculation information such as frequency, observation angles, and excitation conditions.

The user-input data is appended to the geometry file and written in a format that is recognizable to PATCH. Upon execution, the Naval Postgraduate School (NPS) version of PATCH (which has been modified from the original) looks for a file named "inpatch" in the same directory. It performs the required calculations and generates an ASCII output file named "outpatch" which contains all of the output data in readable form. An output file of current coefficients is also generated.

3. PATCH Code Capabilities

Apart from building the shape, PATCH provides some options to the user, one of which is the symmetry option. This option enables the user to reduce the number of computations and thus the time required, by using image planes placed on the $x=0$, $y=0$ or $z=0$ planes. These image

planes can be either perfect electric conductors (PEC) or perfect magnetic conductors (PMC). Other quantities such as voltage sources or distributed impedance follow the image properties and are taken into account automatically. The code capabilities are summarized in Table 1.

PATCH also has the option of entering the number of impedance loads, faces with surface impedance loads and computing the field at near observation points. All these options make the PATCH code a powerful and useful tool in the calculation of RCS for a variety of structures.

Table 1. Summary of PATCH Capabilities

Arbitrary Shape

Open/Closed objects
 Modeled by triangular "patches"
 Variable patch density
 Front end for graphical composition
 Arbitrary edge multiplicity
 Non-orientable surfaces
 Symmetry planes may be included
 Multiple bodies

Surface

Basis functions yield surface currents
 Type: Wilton Rau
 Free of line and point charges
 Equivalent Thevenin circuits
 Lumped and surface impedance loading

Excitation

Voltage sources
 Plane waves
 Both

Calculated Quantities

Surface currents
 Far field patterns
 Radar cross section
 Field calculations at general observation points

Frequency Domain

Pattern loops
 Frequency loops

B. ACAD

The geometry preprocessor BUILD is only capable of simple shapes such as plates, cylinders, cones, and spheres. For computational EM codes to be practical engineering

tools, an efficient surface meshing operation must be available.

The Advanced Computer Aided Design (ACAD) [7,8] application is capable of performing the desired auto-meshing. Databases from other CAD programs can be imported into ACAD and then meshed and output in a special "facet" format. The facet file is ASCII and contains the node and facet information required by PATCH, although it is not in the proper format. An ACAD-to-PATCH translator was written to reformat the facet file into one that is recognized by PATCH. The relationships between codes are summarized in Figure 8.

ACAD provides users with the ability to create and modify geometry in two or three dimensions. Users can choose to model geometry with wireframes, surfaces, or solids. Data entry to ACAD is accomplished through one of many input modes available to the designer. ACAD models can be viewed orthographically or perspective. Users can specify view orientation and choose to display geometry in multiple window configurations. Window operations such as panning, zooming, and auto extents are accomplished at any time providing instream capability. The ACAD user can also control the display of surfaces or solids with options as wireframe, hidden line removal, flat, or Gouraud shading.

At the heart of the ACAD system is the associative database. In an associative database, geometry is linked

together in a relational structure that remembers parent/child dependencies. This type of database enables rapid modifications of geometry, since modifying one geometric element automatically adjusts its dependencies based on a set of predefined rules. For instance, changing an edge of a wing will automatically regenerate any surface(s) built with the edge spline. In turn, all geometry that is associated with the modified wing (i.e., plane/curve and surface intersections, fillets) will automatically regenerate.

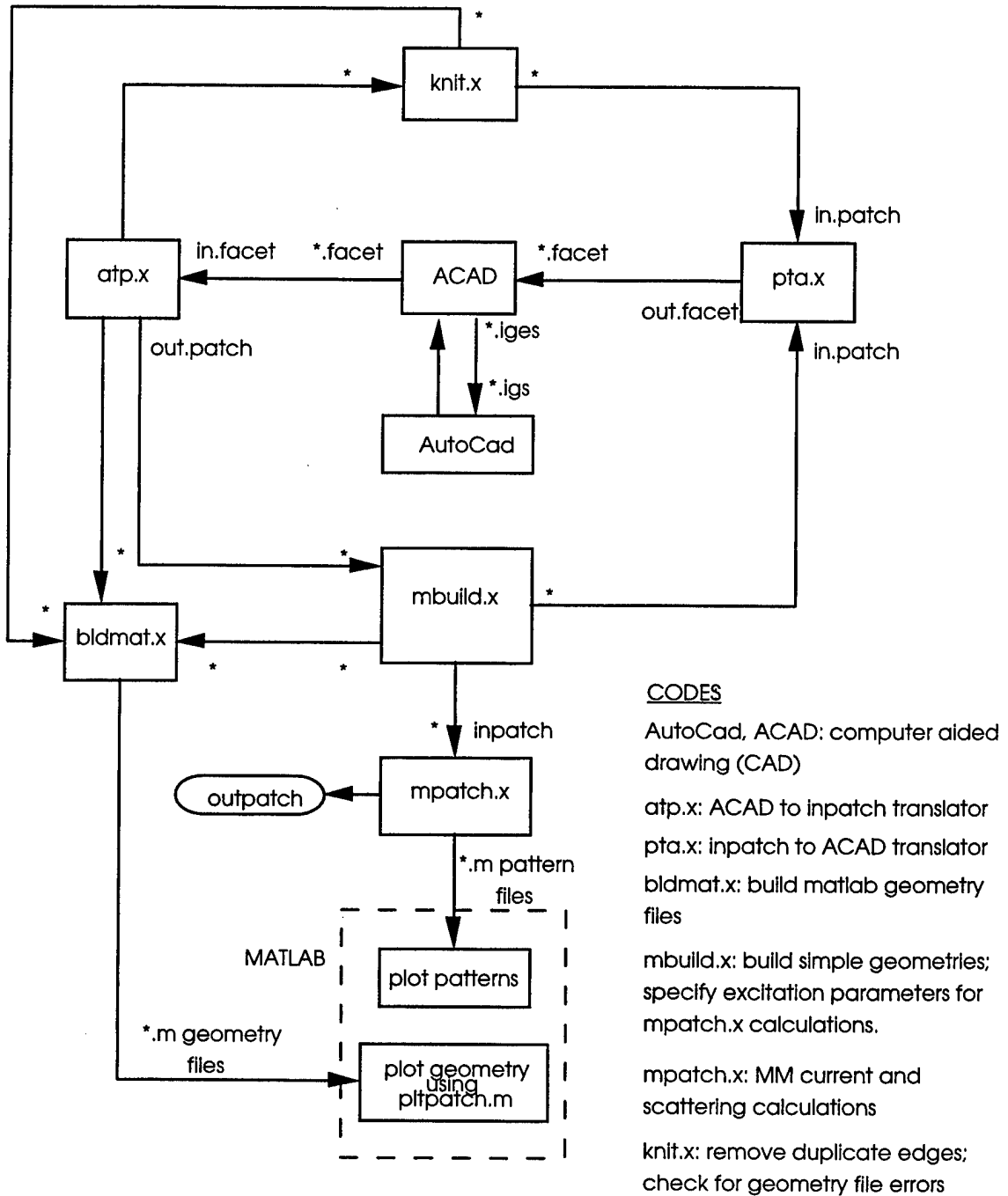
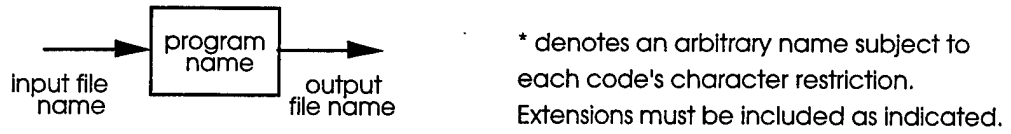


Figure 8. Flow chart illustrating the relationships between the various computer codes (from [6]).

V. RESULTS AND ANALYSIS

It is hypothesized that further reduction of the RCS beyond that obtained by orienting the surface can be achieved by means of the geometric control of discontinuities using serrated edges. Although the use of serrated edges for RCS reduction can be clearly seen on the Northrop B-2 aircraft shown in Figure 1, and was mentioned in several papers and references [1,2], not much data on the reduction magnitude, the associated geometry, or the design methodology are available in the open literature. Parameters of interest include the number of basic serration cells (triangles) required per wavelength, and the aspect ratio of the triangles that form the zig zags.

In order to analyze and verify the effectiveness of serration in RCS reduction, an infinitely thin metallic plate in the x - y plane is considered. The RCS of such a plate with serrated edges is computed and compared against the RCS of a plate of the same size without serrated edges.

To avoid early detection by an enemy's radar, the RCS contributions from a LO aircraft at low grazing angles are particularly important, and have to be as low as possible. Translating this consideration to a thin metallic plate in the x - y plane, analysis is focused at angles in the vicinity of $\theta = \pm 70^\circ$. The infinitely thin assumption is

valid if the wing of the aircraft, which is represented by the plate, is thin compared to the wavelength. Supersonic aircraft tend to have thinner wings than subsonic aircraft.

A. SINGLE-EDGE SERRATED PLATE

Analysis was first performed with serration applied to only one side of the infinitely thin metallic plate. The generic geometry of such a plate is given in Figure 9, where a is the dimension of the plate along the x -axis, b is the dimension of the plate along the y -axis, c is the dimension of the serrated edge along the y -axis, and M is the number of serration cells within a . All of the dimensions are specified in terms of λ .

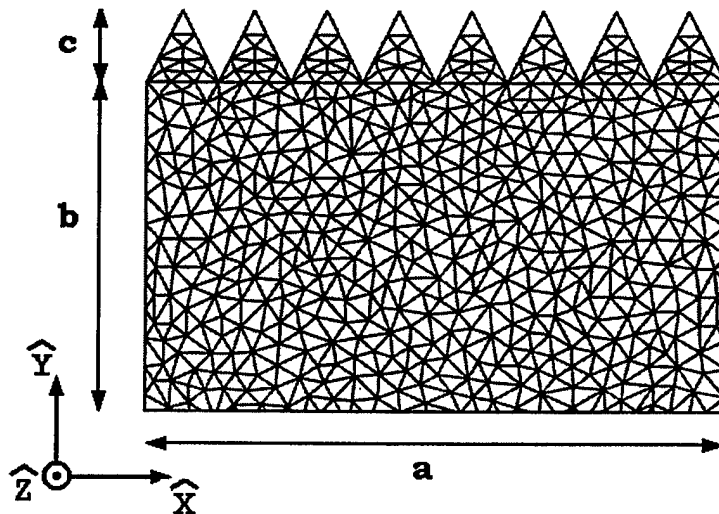


Figure 9. Geometry of an infinitely thin metallic plate in the x - y plane, with isosceles triangular serrated edges.

Based on the geometry given in Figure 9, a RCS reduction of about 10 dB can be attained for vertical polarization at angles around $\theta = -70^\circ$ to -90° . The results are shown in Figures 10 and 11. The serrations applied to the trailing edge successfully reduced the backscattering due to surface traveling waves. However, no significant reduction is observed in the case of horizontal polarization.

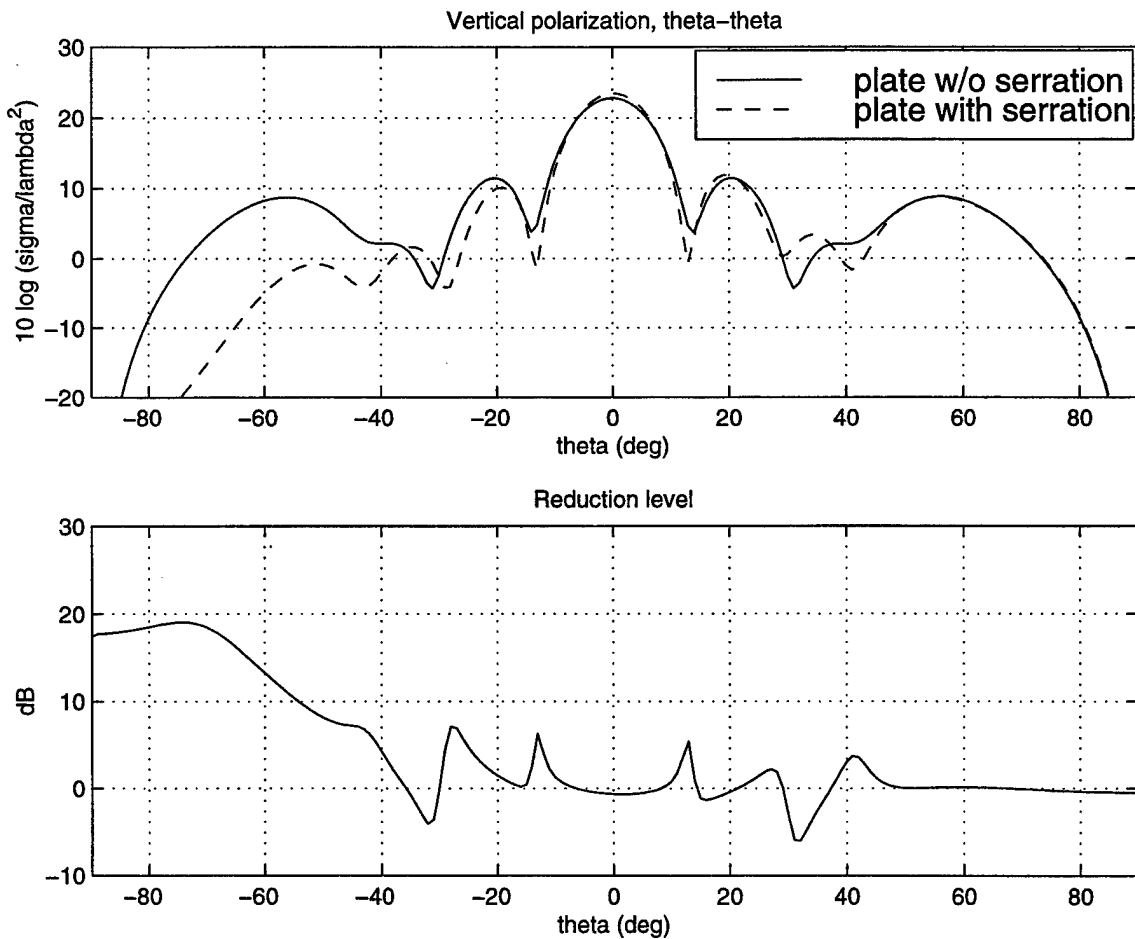


Figure 10. RCS and reduction level with $a=2\lambda$, $b=2\lambda$, $c=0.25\lambda$ and $M=2$.

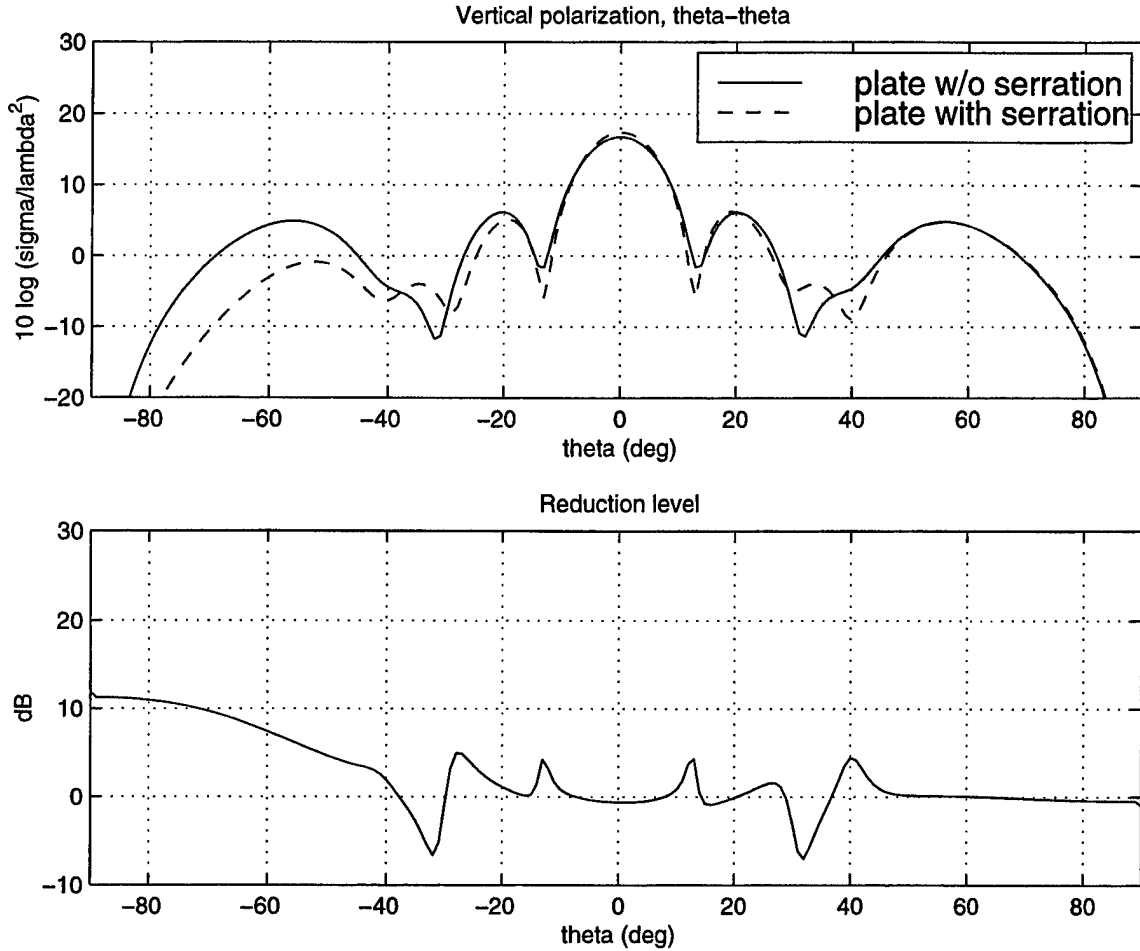


Figure 11. RCS and reduction level with $a=\lambda$, $b=2\lambda$, $c=0.5\lambda$ and $M=1$.

After an inspection of the results for the geometry of Figure 9, variations in the serration shape were examined to obtain improvement in the RCS for horizontal polarization. This may be possible if the number of edges can be reduced without reducing the number of serrations M . This is based on the assumption that the RCS in the transverse plane due to diffractions from the edges may be reduced if the number of edges is reduced. This can be accomplished by using

to diffractions from the edges may be reduced if the number of edges is reduced. This can be accomplished by using right-angle triangular edges instead of isosceles triangular edges, as shown in the generic geometry given in Figure 12.

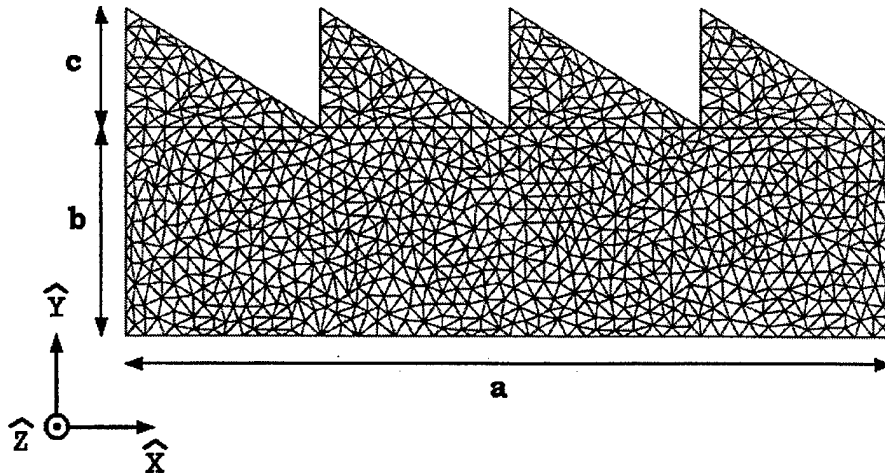


Figure 12. Geometry of an infinitely thin metallic plate in the x - y plane, with right-angle triangular serrated edges.

Based on the geometry shown in Figure 12, and with reference to the results given in Figures 13 and 14, significant RCS reduction in the case of horizontal polarization was achieved with the serration applied at the leading edge. The amount of reduction from $\theta = 70^\circ$ to 90° is kept well above 20 dB. At certain angles, the reduction can be as high as 32 dB. In the case of vertical polarization,

reduction level is greater than 10 dB around $\theta = -70^\circ$ to -90° , as shown in Figures 15 and 16.

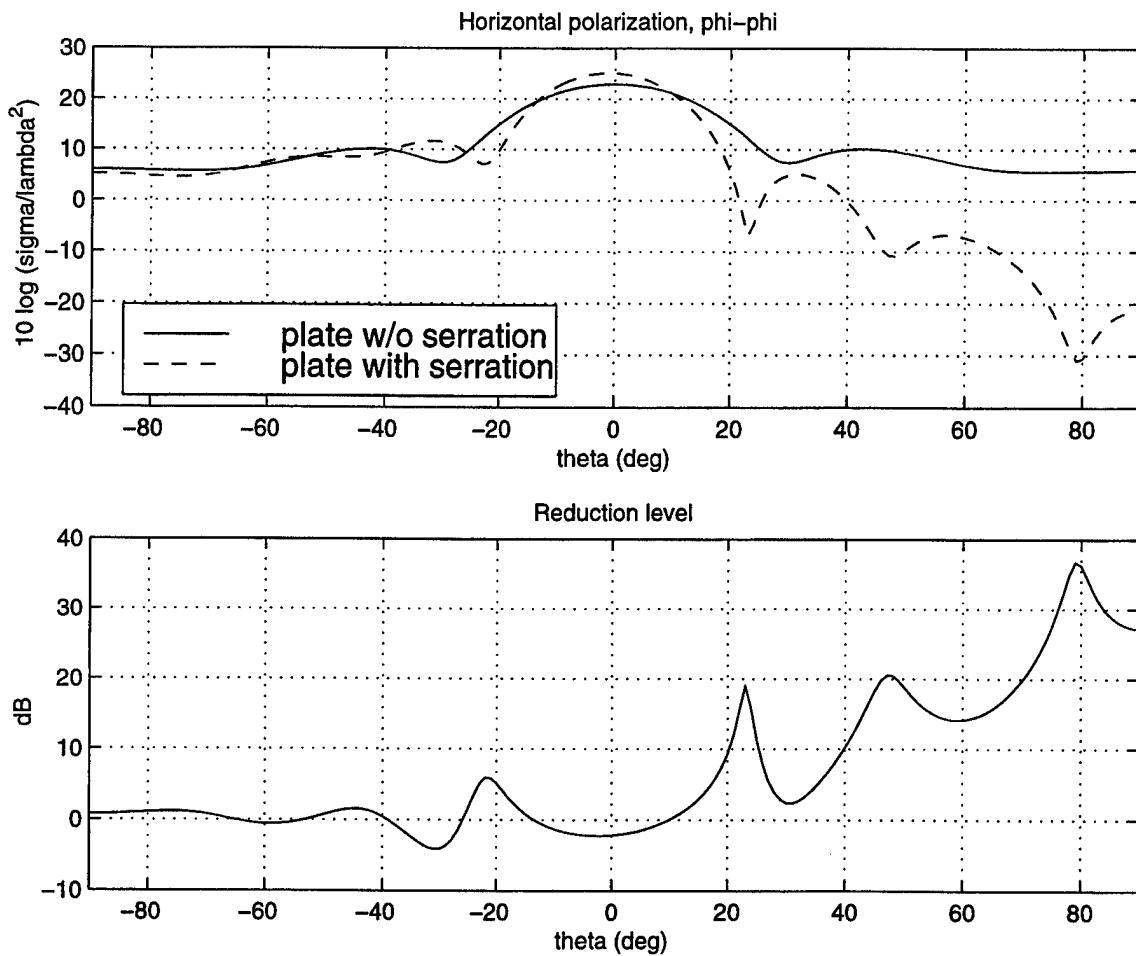


Figure 13. RCS and reduction level, where $a=4\lambda$, $b=\lambda$, $c=0.5774\lambda$ and $M=4$.

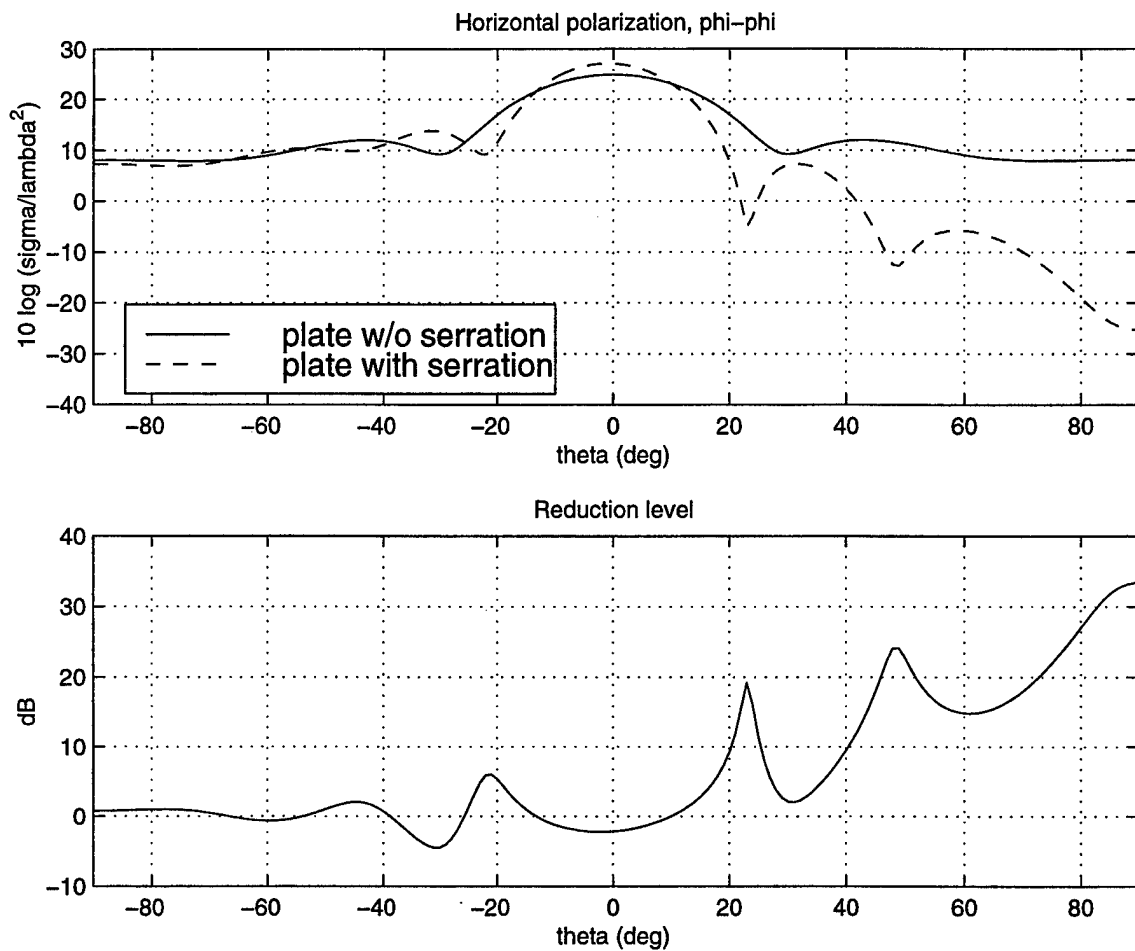


Figure 14. RCS and reduction level, where $a=5\lambda$, $b=\lambda$, $c=0.5774\lambda$ and $M=5$.

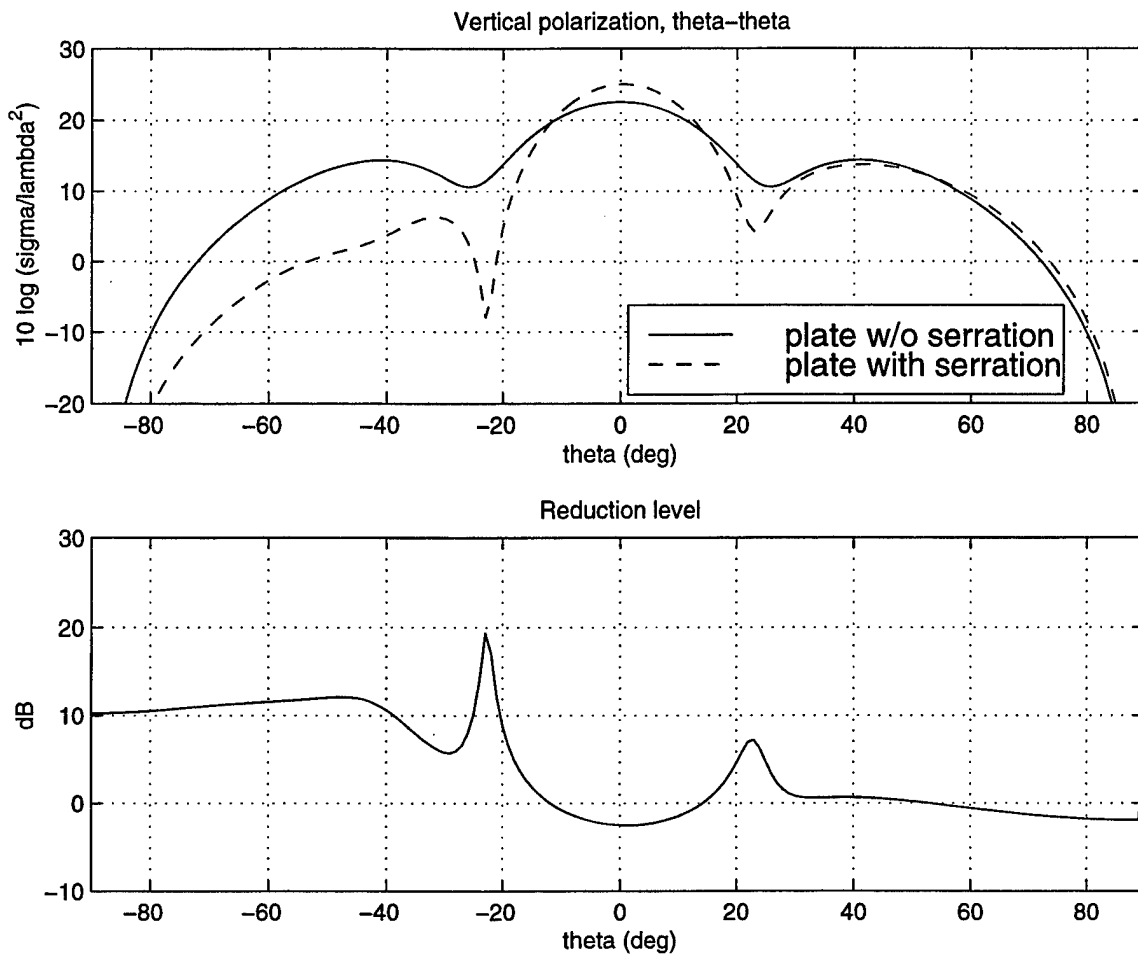


Figure 15. RCS and reduction level, where $a=4\lambda$, $b=\lambda$, $c=0.5774\lambda$ and $M=4$.

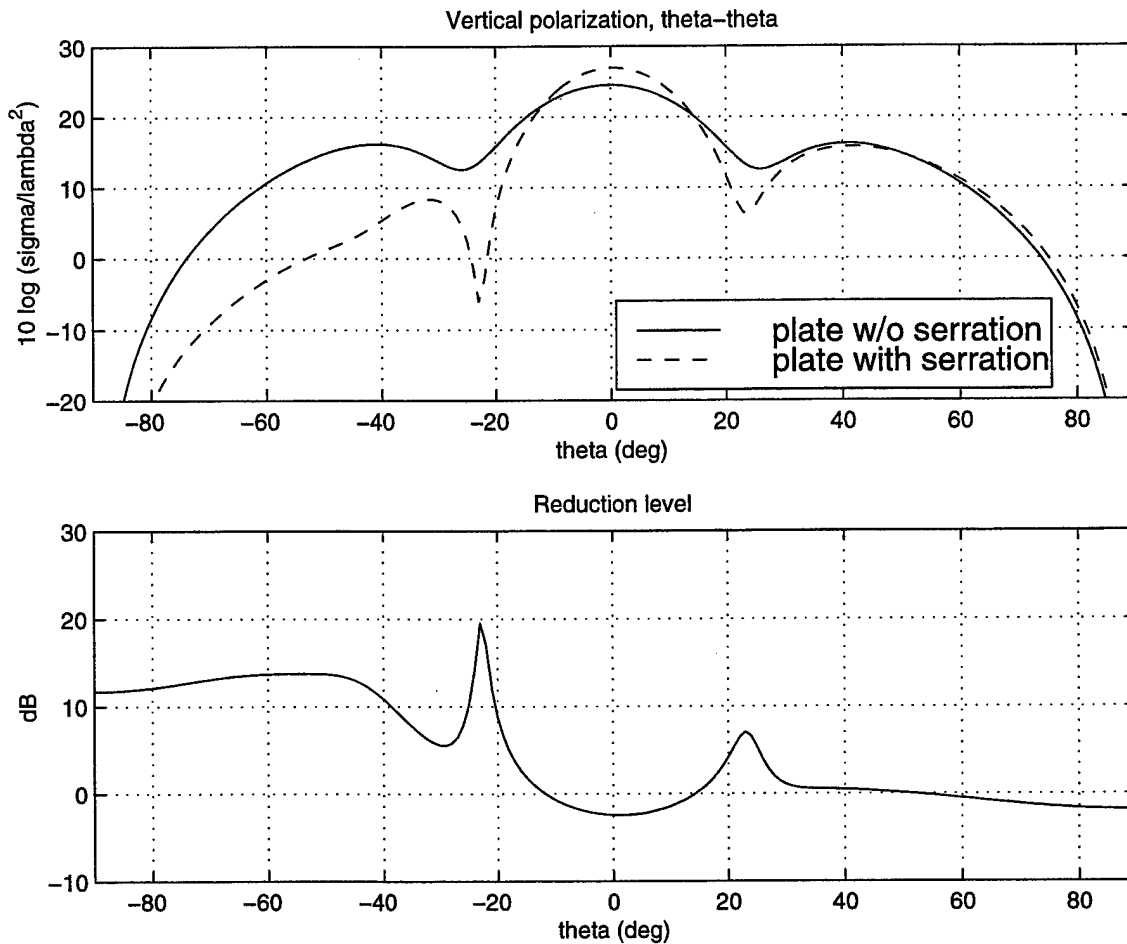


Figure 16. RCS and reduction level, where $a=5\lambda$, $b=\lambda$, $c=0.5774\lambda$ and $M=5$.

In the case of the vertical polarization, reduction is achieved by applying the serration at the trailing edge. The serrated edges effectively reduced the RCS contributions due to surface traveling waves. As for the horizontal polarization, reduction is achieved by applying the serration at the leading edge. The serrated edges reduced

the RCS contributions due to edge diffraction in the transverse plane.

In order to investigate an overall reduction for both vertical and horizontal polarizations, the design of a double-edge serrated plate is considered in the next phase of analysis.

B. DOUBLE-EDGE SERRATED PLATE

With reference to the results obtained based on the geometries shown in Figures 9 and 12, a double-edge serrated plate was created to investigate the RCS reduction for both vertical and horizontal polarizations. To reduce RCS reduction in the case of horizontal polarization, right-angle triangular edges are applied at the leading edge. As for the case of vertical polarization, isosceles triangular edges are applied at the trailing edge. The generic geometry of such a double-edge serrated plate is shown in Figure 17.

RCS reduction for both polarizations was achieved with the geometry given in Figure 17. The results are shown in Figures 18 and 19. However, note that the reduction level provided by the double-edge serrated plate, for either the vertical or horizontal polarization, is less than that provided by the single-edge serrated plate. Reduction in both polarizations is possible with the double-edge serrated plate, whereas the larger reduction in magnitude for a single polarization occurs with the single-edge serrations.

Hence the application of serrated edges is a compromise, and it depends on the specific mission profile of the LO aircraft and the threat radar's polarization.

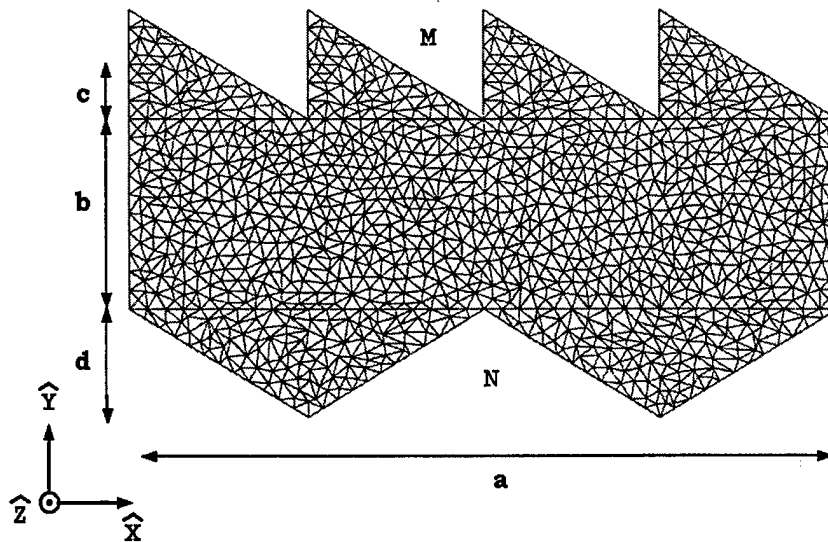


Figure 17. Geometry of an infinitely thin metallic plate in the x - y plane, with double-edge serrations; right-angle triangular serrated edges applied at the leading edge and isosceles triangular edges applied at the trailing edge.

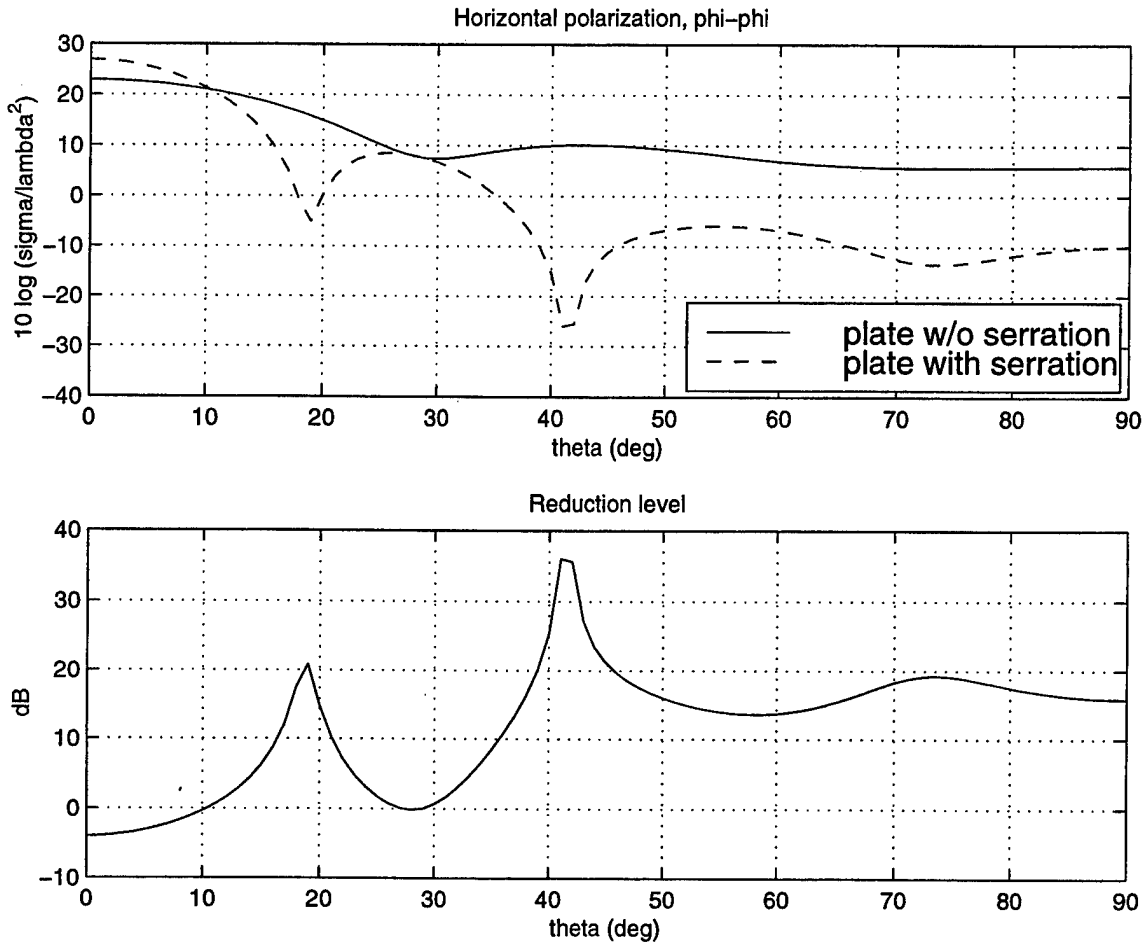


Figure 18. RCS and reduction level where $a=4\lambda$, $b=\lambda$, $c=0.5774\lambda$, $d=0.5774\lambda$, $M=4$ and $N=0.5\lambda$.

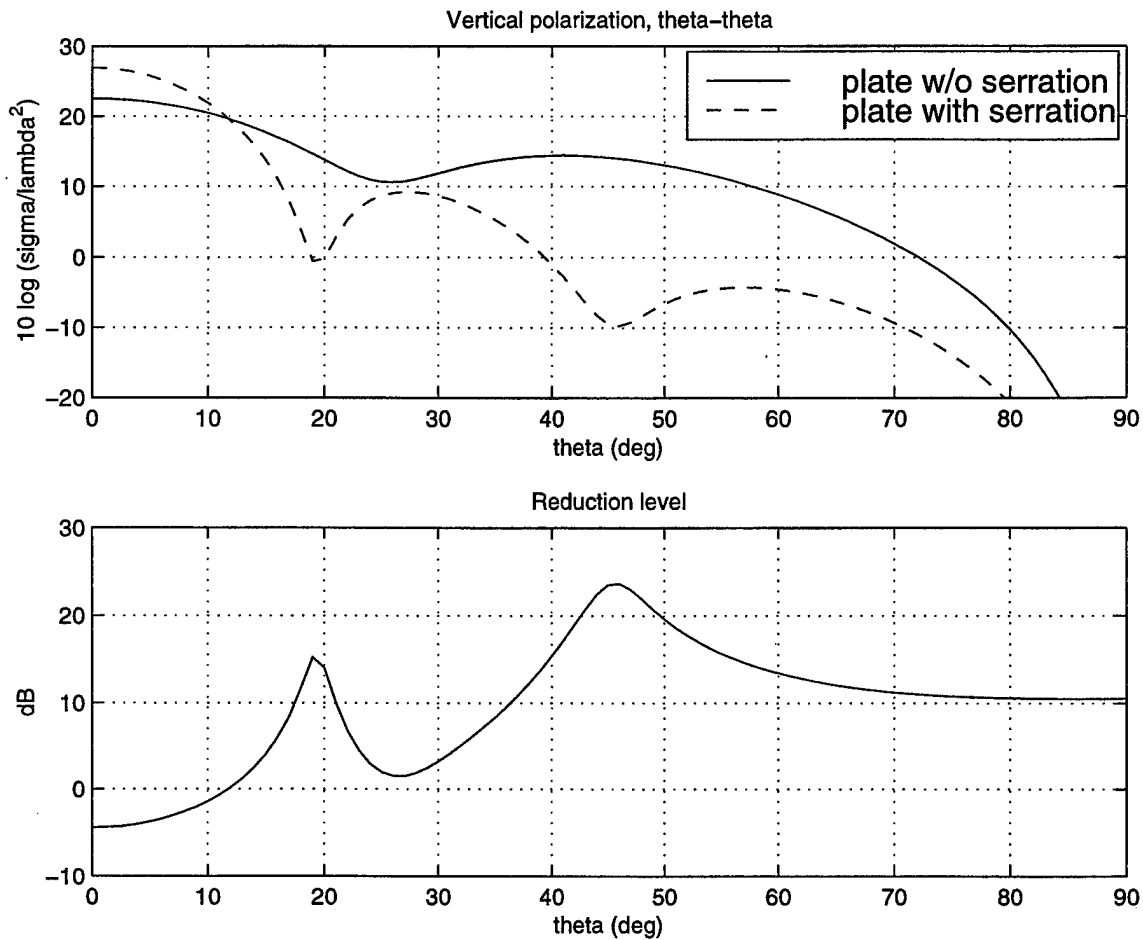


Figure 19. RCS and reduction level where $a=4\lambda$, $b=\lambda$, $c=0.5774\lambda$, $d=0.5774\lambda$, $M=4$ and $N=0.5\lambda$.

VI. CONCLUSIONS

The four basic techniques typically employed in radar cross section reduction, namely shaping, surface material selection, active and passive cancellation, have been discussed in Chapter I. The significance of edge scattering to the case of LO platforms has also been discussed. The edge serration method can be considered as a combination of shaping and passive cancellation. The concept of two major scattering mechanisms related to edges, namely surface traveling waves and edge diffraction, have been explained. The three most commonly used high-frequency techniques for predicting scattering from metallic edges (GTD, PTD and the method of equivalent currents) have been presented. Although the approximate high-frequency methods were not used to compute the RCS of the plates in this research, they provide a method for predicting the location and level of edge-scattered fields. Furthermore, the ray model provides some physical insight into the behavior of diffracted fields. These analytical techniques are generally used for edges that are 5 to 10λ or greater in length, although they can still give useful results for edges as short as 1 or 2λ .

The objective of this thesis is to investigate and evaluate the effectiveness of RCS reduction by means of the geometric control of discontinuities through serrated edges.

The results and analysis have been presented in Chapter V. It has been known for sometime that the use of relatively large serrated edges (i.e., about 10λ) is an effective means of RCS reduction. Such application can be seen on the zig zag trailing edge of the Northrop B-2 and the Lockheed F-117A aircraft. Of particular interest in this research is the effectiveness of relatively short edge serrations in the reduction of the principal plane RCS. Because of the short edge lengths, the method of moments was used to compute the surface current and scattered field. The results obtained show that significant RCS reduction for low grazing angles is achievable with smaller serrated edges (i.e., about 1λ per serration cell).

The potential of RCS reduction by means of the geometric control of discontinuities using serrated edges has been clearly demonstrated. In practice, the serrations would probably be applied to the surface of the wing as illustrated in Figure 20. Most modern aircraft are constructed from composite materials, which are non-conducting. A layer of conducting foil can be laid over the composite structure. The conductor would also provide electromagnetic shielding for the internal aircraft parts.

Further research should be conducted to determine the bandwidth of the RCS reduction. By performing several calculations at frequencies above and below the design

frequency, an effective bandwidth of the treatment can be obtained. Finally, the spatial distributions of the diffracted fields are also interesting. This research only examined the diffracted field in the principal planes. The reduction of RCS in one direction is generally accompanied by an increase in other directions unless cancellation or absorption has occurred. A contour plot of RCS would provide information on the redistribution of the scattered field.

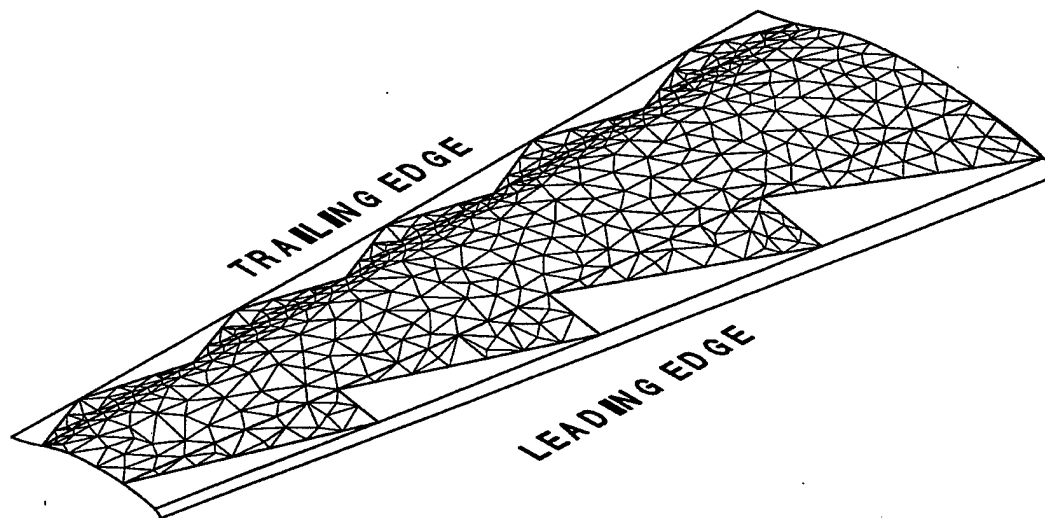


Figure 20. Serrated edges applied to the surface of an aircraft's wing.

LIST OF REFERENCES

1. Jenn, D. C., *Radar and Laser Cross Section Engineering*, AIAA Education Series, AIAA, Washington, DC, 1995.
2. Knott, E. F., J. F. Shaeffer and M. T. Tuley, *Radar Cross Section*, Artech House, Boston, 1993.
3. Keller, J. B., "Diffraction by an Aperture," *J. App. Phys.*, Vol. 28, No. 4, April 1957, pp. 426-444.
4. Michaeli, A., "Equivalent Edge Currents for Arbitrary Aspects of Observation," *IEEE Trans. on Antennas and Propagation.*, Vol. AP-32, No. 3, March 1984, pp. 252-258. See also correction in Vol. Ap-33, February 1985, pp. 227.
5. Knott, E. F., T. B. A. Senior, "Comparison of Three High-Frequency Diffraction Techniques," *Proc. IEEE*, Vol. 62, No. 11, November 1974.
6. Johnson, W., *Patch Code Users' Manual*, Sandia Report SAND87-2991, May 1988.
7. *The ACAD User's Manual*, Lockheed Martin Corp., Ft. Worth, April 1995.
8. *ACAD Reference Set - Volume 1*, Lockheed Martin Corp., Ft. Worth, April 1995.
9. Marhefka, R. J., *Radar Cross Section - Basic Scattering Code, RCS-BSC (Ver. 2.0) User's Manual*, The Ohio State University, ElectroScience Laboratory, Technical Report 718295-15, February 1990.
10. Ufimtsev, P. Ia., "Approximate Computation of the Diffraction of Plane Electromagnetic Waves at Certain Metal Bodies: Pt. I. Diffraction Patterns at a Wedge and a Ribbon," *Zh. Tekhn. Fiz. (USSR)*, Vol. 27, No. 8, 1957, pp. 1708-1718.
11. Sommerfeld, A., "Rmathematische Theorie der Diffraction," *Math Ann.*, Vol. 47 1896, pp. 317-374.

INITIAL DISTRIBUTION LIST

	No. of Copies
1. Defense Technical Information Center2 8725 John J. Kingman Rd., STE 0944 Ft. Belvoir, Virginia 22060-6218	
2. Dudley Knox Library.....2 Naval Postgraduate School 411 Dyer Rd. Monterey, California 93943-5101	
3. Chairman, Code EC.....1 Department of Electrical and Computer Engineering Naval Postgraduate School Monterey, California 93943-5121	
4. Professor David C. Jenn, Code EC/Jn.....2 Department of Electrical and Computer Engineering Naval Postgraduate School Monterey, California 93943-5121	
5. Professor Phillip A. Pace, Code EC/Pc.....1 Department of Electrical and Computer Engineering Naval Postgraduate School Monterey, California 93943-5121	
6. Head, Department of Strategic Studies.....1 SAFTI Military Institute Ministry of Defence 500 Upper Jurong Road S(638364) Singapore	
7. Mr Matthew K.M. Yong.....2 Naval System Division Defence Materiel Organisation Ministry of Defence 18 th Storey, Tower A Defence Technology Towers Depot Road, S(0410) Singapore	